

# Electrochemically Tunable Magnetic Phase Transition in a High- $T_c$ Chromium Cyanide Thin Film

O. Sato, T. Iyoda, A. Fujishima,\* K. Hashimoto\*

Molecular-based ferrimagnetic thin films with high critical temperatures ( $T_c$ ) composed of mixed-valence chromium cyanides were synthesized by means of a simple electrochemical route. The highest  $T_c$  was 270 K, obtained for  $\text{Cr}_{2.12}(\text{CN})_6$ . The  $T_c$  values were easily controlled by changing the preparation conditions. Moreover, a reversible shift of  $T_c$  could be electrochemically induced. As a result of such electrochemical control, these cyanides can be switched reversibly back and forth between ferrimagnetism and paramagnetism. These magnets thus represent materials in which magnetic properties are combined with electrical functions.

There has been great interest in the study of the magnetic properties of molecular-based compounds (1–6). One of the main challenges in this field is the design of materials with high critical temperatures. To facilitate the development of future recording and switching devices, it would be desirable to be able to control the magnetic phase transition through electrical or optical stimuli, which has never been achieved in conventional magnets. We set out to prepare high- $T_c$ , electrochemically tunable, metal complex-based magnets. Metal cyanides were used as molecular building blocks for two reasons: (i) electrochemical reduction can be applied to the synthesis of cyanide magnetic films consisting of mixed-valence transition metals (7), which provides a way of controlling the structure of the film by means of the electrode potential and thereby potentially raising  $T_c$  (8), and (ii) the oxidation states of the metal ions constituting the films can be electrochemically controlled by making use of their zeolitic properties and their thin film form as opposed to powder form, allowing modification of their magnetic properties after preparation. Through the use of this approach, ferrimagnets with various linkage structures and different  $T_c$  values were obtained as thin films. The maximum  $T_c$  obtained by optimization of the electrochemical conditions was 270 K, one of the highest  $T_c$  values obtained for molecular-based magnets to date (8, 9). In addition, we succeeded in inducing a reversible, mag-

netic phase transition electrochemically. Mixed-valence chromium cyanides, which are Prussian blue analogs, are usually obtained as fine powders by means of the reaction of substitution-inert  $[\text{Cr}^{\text{III}}(\text{CN})_6]^{3-}$  with labile  $\text{Cr}^{\text{II}}$ . In the electrochemical technique, on the other hand, a labile chemical species is generated by electrochemical reduction in an aqueous solution of the substitution-inert  $\text{K}_3\text{Cr}(\text{CN})_6$  (10) and  $\text{CrCl}_3$ . Insoluble polynuclear chromium cyanides are thus deposited on an electrode surface as thin films. In this study, the electrochemical reduction was performed between  $-840$  and  $-760$  mV versus a saturated calomel electrode (SCE). The working, counter, and reference electrodes were  $\text{SnO}_2$ , Pt, and SCE, respectively. Thin films of various colors were obtained depending on the electrode potential. Because the stoichiometric composition of these magnetic materials strongly depended on the preparation conditions, three typical materials [referred to as (a), (b), and (c)] are described here. These species were prepared at (a)  $-840$  mV in the absence of CsCl, (b)  $-760$  mV in the absence of CsCl, and (c)  $-760$  mV in the presence of CsCl.

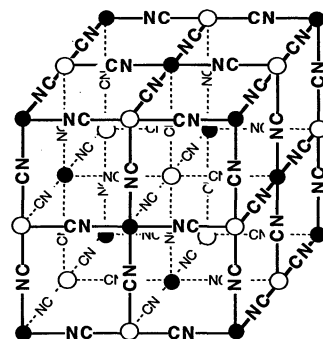


**Fig. 1.** Unit cell of mixed-valence chromium cyanide: (○)  $\text{Cr}^{\text{II/III}}$  ( $\text{Cr}^{\text{I}}$  or  $\text{Cr}^{\text{II}}$ ); (●)  $\text{Cr}^{\text{III}}$  ( $\text{Cr}^{\text{III}}$  or  $\text{Cr}^{\text{II}}$ ). The three materials a, b, and c described in the text differed in how CN was coordinated (see Fig. 2). Water molecules and interstitial ions in the unit cell were omitted for clarity.

Elemental analysis showed their composition to be (a)  $\text{Cr}_{2.43}(\text{CN})_6 \cdot 6.09\text{H}_2\text{O}$  [ $\text{Cr}_{1.29}^{\text{II}}\text{Cr}_{1.14}^{\text{III}}(\text{CN})_6$  from charge balance]; (b)  $\text{Cr}_{2.12}(\text{CN})_6 \cdot 2.80\text{H}_2\text{O}$  [ $\text{Cr}_{0.36}^{\text{II}}\text{Cr}_{1.76}^{\text{III}}(\text{CN})_6$ ]; and (c)  $\text{Cs}_{1.15}\text{Cr}_{2.06}(\text{CN})_6 \cdot 1.78\text{H}_2\text{O}$  [ $\text{Cs}_{1.15}\text{Cr}_{1.33}^{\text{II}}\text{Cr}_{0.73}^{\text{III}}(\text{CN})_6$ ] (11). The x-ray diffraction patterns of the three materials were qualitatively consistent with the typical structure of three-dimensional, mixed-valence transition metal cyanides, that is, a face-centered-cubic structure (Fig. 1). The lattice parameters for (a), (b), and (c) were 10.41, 10.44, and 10.39 Å, respectively. The infrared (IR) spectra of the materials (Fig. 2) were analyzed to gain insight into the Cr-CN coordination: (a) contained only  $\text{Cr}^{\text{III}}\text{-CN}$ , (c) contained only  $\text{Cr}^{\text{II}}\text{-CN}$ , and (b) contained both  $\text{Cr}^{\text{III}}\text{-CN}$  and  $\text{Cr}^{\text{II}}\text{-CN}$  (12). Changing the reduction potential from  $-840$  toward  $-760$  mV in steps of 20 mV generally resulted in an increase in the fraction of the  $\text{Cr}^{\text{II}}\text{-CN}$  moiety. Note that the structure of (a) is similar to that of the material reported by Mallah *et al.* (4) as a powder sample (8) and that the structure of (c) can be classified as a linkage isomer of (a).

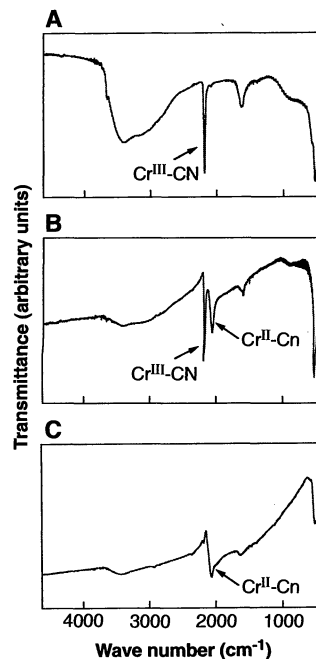


**Fig. 2.** IR spectra of materials (a), (b), and (c).  $\text{Cr}^{\text{III}}\text{-CN}$  and  $\text{Cr}^{\text{II}}\text{-CN}$  indicate that the IR peaks correspond to the stretching modes of CN in the  $\text{Cr}^{\text{III}}\text{-CN}$  moiety ( $\text{Cr}^{\text{III}}$  is coordinated to carbon) or the  $\text{Cr}^{\text{II}}\text{-CN}$  moiety ( $\text{Cr}^{\text{II}}$  is coordinated to carbon), respectively. The CN stretching bands are located at (A) 2187  $\text{cm}^{-1}$  ( $\text{Cr}^{\text{III}}\text{-CN}$ ) [material (a)], (B) 2186  $\text{cm}^{-1}$  ( $\text{Cr}^{\text{III}}\text{-CN}$ ) and 2071  $\text{cm}^{-1}$  ( $\text{Cr}^{\text{II}}\text{-CN}$ ) [material (b)], and (C) 2063  $\text{cm}^{-1}$  ( $\text{Cr}^{\text{II}}\text{-CN}$ ) [material (c)]. The OH stretching and bending modes of  $\text{H}_2\text{O}$  are observed around 3400 and 1600  $\text{cm}^{-1}$ , respectively. Because of the broad absorption band in (B) and (C) ranging from near-IR to IR, the OH and CN stretching modes are superimposed on the edge of the absorption. The spectra show that the type of Cr-CN coordination can be controlled via variation of the preparation conditions.

O. Sato and T. Iyoda, Kanagawa Academy of Science and Technology, Tokyo Institute of Polytechnics, 1583 Iiyama Atsugi, Kanagawa 243-02, Japan.  
A. Fujishima, Department of Applied Chemistry, The University of Tokyo, 7-3-1 Hongo Bunkyo-ku, Tokyo 113, Japan.  
K. Hashimoto, Kanagawa Academy of Science and Technology, Tokyo Institute of Polytechnics, Kanagawa 243-02, and Department of Applied Chemistry, The University of Tokyo, 7-3-1 Hongo Bunkyo-ku, Tokyo 113, Japan.

\*To whom correspondence should be addressed.

Magnetic properties were investigated with a superconducting quantum interference device magnetometer (Quantum Design MPMS-5S). For all of the materials, as the temperature was lowered, the product of the magnetic susceptibility and temperature,  $\chi_m T$ , smoothly decreased, reached a minimum, and then increased again at lower temperatures. This type of behavior is an indication of ferrimagnetism, with short-range antiferromagnetic interactions between nearest neighbor chromium ions and noncompensation of their spins. The  $\chi_m^{-1}$  versus  $T$  plots became linear in the paramagnetic region and could be fit to the equation,  $\chi_m^{-1} = (T - \theta)/C$ . The Curie constants  $C$  for (a), (b), and (c) were 4.58, 4.14, and 4.03  $\text{cm}^3 \text{mol}^{-1} \text{K}$ , respectively, and the Weiss constants  $\theta$ , which reflect the magnitude of the antiferromagnetic interaction between the chromium ions, were  $-320$ ,  $-416$ , and  $-119$  K, respectively. Plots of field-cooled magnetization (FCM) versus temperature at magnetic field  $H = 5$  G (Fig. 3) displayed abrupt breaks at  $T_c = 240$ , 270, and 150 K for (a), (b), and (c), respectively. The field dependence of the magnetization for up to 5 T was measured at  $T = 10$  K. This yielded magnetizations at 5 T of about 0.7, 0.5, and 0.7 Bohr magnetons ( $\mu_B$ ) per  $\text{Cr}_{2.43}(\text{CN})_6$  (a),  $\text{Cr}_{2.12}(\text{CN})_6$  (b), and  $\text{Cs}_{1.15}\text{Cr}_{2.06}(\text{CN})_6$  (c), respectively (13). The magnetic hysteresis loops obtained at 5 K yielded remnant magnetizations ( $M_r$ ) of 1204, 1130, and 1290  $\text{cm}^3 \text{mol}^{-1} \text{G}$  and coercive fields ( $H_c$ ) of 25, 143, and 130 G, respectively. These results showed that the thin films prepared electrochemically were ferrimagnets with high values of  $T_c$  and that their magnetic properties could be varied drastically with small changes in the electrochemical preparation conditions.

The characteristic difference between material (b), with  $T_c = 270$  K, and the other magnets with lower  $T_c$  that were prepared in the absence of CsCl is the abundance of Cr and  $\text{H}_2\text{O}$  in the unit cell; the amount of Cr (or  $\text{Cr}^{\text{III}}$ ) in (b) was relatively

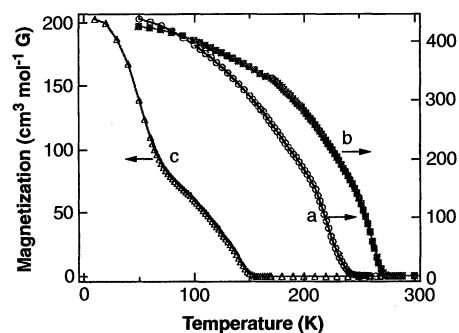
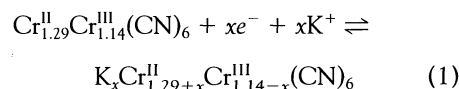


**Fig. 3.** Curves of FCM versus temperature at  $H = 5$  G for material (a),  $T_c = 240$  K; material (b),  $T_c = 270$  K; and material (c),  $T_c = 150$  K.

large, whereas the water content was small (11). The larger amount of Cr in the unit cell increased the number of nearest neighbor Cr ions and also suggests that the number of  $\text{Cr}(\text{CN})_6$  vacancies, which inhibit the magnetic interactions between Cr atoms, was reduced. The average numbers of magnetic neighbors in (a) and (b) were 4.9 and 5.7, respectively. In other words, the vacancies of  $[\text{Cr}^{\text{II}}(\text{CN})_6]^{4-}$  or  $[\text{Cr}^{\text{III}}(\text{CN})_6]^{3-}$ , which are indispensable for charge compensation, could be eliminated in (b) through the generation of the large amount of  $\text{Cr}^{\text{III}}$  ( $\text{Cr}^{\text{III}}\text{-CN-Cr}^{\text{III}}$  moiety) with its comparatively high positive charge. Because  $T_c$  rises with the number of magnetic neighbors, material (b) had a higher  $T_c$  than did the other magnets. The reduced water content in (b) is consistent with the decrease of the  $\text{Cr}(\text{CN})_6$  vacancies. A more detailed explanation will require additional data.

The electrochemical properties were investigated to study whether the magnetic phase transition could be controlled electrochemically after the film preparation. The magnetic films prepared were used as working electrodes and were biased from  $-1.2$  to  $1.0$  V versus SCE in 1 M KCl aqueous solution. The redox reactions proceeded reversibly and were accompanied by a color change. Voltammetric peaks were observed at around  $-0.84$  and  $-1.08$  V for both (a) and (b) and at around  $-1.08$  V for

(c). The redox process for (a), for example, could be formulated as follows:



A sharp peak at around  $-0.84$  V corresponded to the reduction of carbon-coordinated  $\text{Cr}^{\text{III}}$ , which resulted in the formation of the  $\text{Cr}^{\text{II}}\text{-CN}$  moiety with low spin. This assignment is consistent with our Fourier transform IR (FT-IR) measurement in situ; the IR peak at  $2187 \text{ cm}^{-1}$  vanished upon reduction, whereas a new peak at  $2071 \text{ cm}^{-1}$  appeared simultaneously (14). The oxidation reaction at anodic potential could not be observed under the present electrochemical conditions. The FCM versus temperature at  $H = 5$  G was measured after reducing  $\text{Cr}^{\text{III}}$  at  $-0.95$  and  $-1.2$  V (Fig. 4). The critical temperatures for (a) and (b) reduced at  $-0.95$  V were about 100 and 150 K, respectively, and those for (a), (b), and (c) reduced at  $-1.2$  V were all below 100 K. Thus, after reduction at  $-0.95$  V, the critical temperatures dropped by 140 and 120 K for (a) and (b), respectively. The hysteresis loops of (a) and (b) yielded  $H_c = 220$  and 370 G at 5 K, respectively. The  $H_c$  values increased after the reduction at  $-1.2$  V to  $H_c = 550$  G for (a), 700 G for (b), and 530 G for (c). This behavior showed that the magnetic phase transition could be controlled by reversible redox reactions accompanied by  $\text{K}^+$  doping. Consequently, we could regulate the two states, ferrimagnetism and paramagnetism, electrochemically in the tunable temperature range (Fig. 4).

The magnetic and optical behavior described here indicates that the materials prepared by means of the reduction route are high- $T_c$  ( $\leq 270$  K), electrochemically tunable magnets. They show magnetic bistability in the sense that at a given temperature they may exhibit either ferrimagnetism or paramagnetism. This study opens up a new route for developing magnets in which magnetic properties are coupled with electrical functions. We regard these new types of magnets as electromagnetic materials (15). Furthermore, considering the electrochromic character of these magnets, our study may be extended to the design of molecular-based magnets with both optical and electrical functions.

## REFERENCES AND NOTES

1. J. S. Miller and A. J. Epstein, *Angew. Chem. Int. Ed. Engl.* **33**, 385 (1994).
2. D. Gatteschi, *Adv. Mater.* **9**, 635 (1994).
3. O. Kahn, D. Gatteschi, J. S. Miller, F. Palacio, Eds., *Magnetic Molecular Materials* (Kluwer, London, 1991), vol. E198.
4. T. Mallah, S. Thiébaud, M. Verdaguer, P. Veillet, *Science* **262**, 1554 (1993).
5. V. Gadet, T. Mallah, J. Castro, P. Veillet, M. Verdaguer, *J. Am. Chem. Soc.* **114**, 9213 (1992).
6. J. M. Manriquez, G. T. Yee, R. S. McLean, A. J.

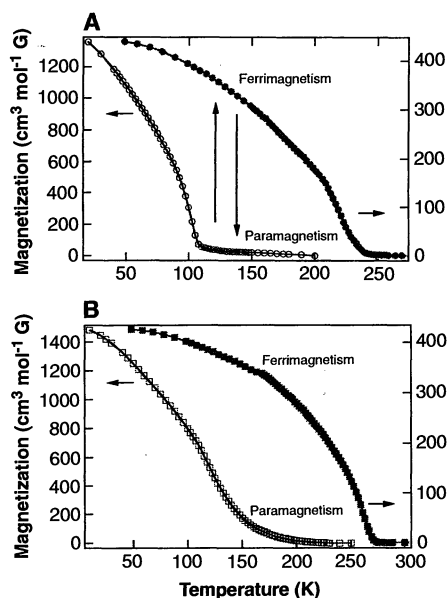


**Fig. 4.** Magnetic bistability induced by the redox reaction of chromium ( $\text{Cr}^{\text{III}}$ ) in (A) material (a) and (B) material (b). The FCM versus temperature curves before electrochemical reduction (solid symbols, right axis) and after electrochemical reduction at  $-0.95$  V (open symbols, left axis). The material (a) can be switched from ferrimagnetism or paramagnetism between 100 and 240 K (A); the material (b) shows such bistability between 150 and 270 K (B).

Epstein, J. S. Miller, *Science* **252**, 1415 (1991).  
 7. K. Itaya, I. Uchida, V. D. Neff, *Acc. Chem. Res.* **19**, 162 (1986).  
 8. The cyanochromate  $[\text{Cr}_5(\text{CN})_{12}] \cdot 10\text{H}_2\text{O}$  with  $T_c = 240\text{ K}$ , reported by T. Mallah *et al.* (4), has the highest  $T_c$  reported for a stable molecular-based magnet before the present work.  
 9.  $\text{V}(\text{TCNE})_2 \cdot 0.5\text{CH}_2\text{Cl}_2$ , reported by J. M. Manriquez *et al.* (6), shows spontaneous magnetization at room temperature but is air-sensitive. The  $T_c$  of 270 K obtained in the present study is the second highest  $T_c$  reported if such air-sensitive magnets are included in the comparison.  
 10. W. B. Schaap, R. Krishnamurthy, D. K. Wakefield, W. F. Coleman, in *Coordination Chemistry*, S. Kirschner, Ed. (Plenum, New York, 1969), pp. 177–206.  
 11. Elemental analysis of the three materials was as follows. (a): C, 17.57%; N, 20.50%; H, 2.97%; and Cr, 30.87%. (b): C, 22.32%; N, 25.65%; H, 1.72%; and Cr, 33.87%. (c): C, 14.98%; N, 16.50%; H, 0.73%; Cr, 21.71%; and Cs, 30.91%. Small amounts of K and Cl were also found in (c). The unit cell formulas of (a), (b), and (c) were  $\text{Cr}_{3.61}^{\text{II}}\text{Cr}_{3.19}^{\text{III}}(\text{CN})_{16.78}[\ ]_{1.20}(\text{H}_2\text{O})_{17.03}$ ,  $\text{Cr}_{1.29}^{\text{II}}\text{Cr}_{6.29}^{\text{III}}(\text{CN})_{21.43}[\ ]_{0.43}(\text{H}_2\text{O})_{10.00}$ , and  $\text{Cs}_{4.34}\text{Cr}_{3.02}^{\text{II}}\text{Cr}_{2.75}^{\text{III}}(\text{CN})_{22.64}[\ ]_{0.23}(\text{H}_2\text{O})_{6.72}$ , respectively, where  $[ ]$  stands for  $\text{Cr}(\text{CN})_6$  vacancies.

Considering the experimental error, the structures corresponding to (a)  $[\text{Cr}_{2.43}(\text{CN})_6 = \text{Cr}_{1.29}^{\text{II}}\text{Cr}_{0.14}^{\text{III}}[\text{Cr}^{\text{III}}(\text{CN})_6]]$  and (c)  $[\text{Cs}_{1.15}\text{Cr}_{2.06}(\text{CN})_6 = \text{Cs}_{1.15}\text{Cr}_{0.33}^{\text{II}}\text{Cr}_{0.73}^{\text{III}}[\text{Cr}^{\text{III}}(\text{CN})_6]]$  were qualitatively consistent with the typical structure  $\text{Cr}_{2.5}(\text{CN})_6 = \text{Cr}_{1.5}^{\text{II}}\text{Cr}^{\text{III}}(\text{CN})_6$  [saturation magnetization expected is  $3\ \mu_B$  per  $\text{Cr}_{2.5}(\text{CN})_6$  and  $\text{CsCr}_2(\text{CN})_6 = \text{CsCr}^{\text{II}}\text{Cr}^{\text{III}}(\text{CN})_6$  [ $1\ \mu_B$  per  $\text{CsCr}_2(\text{CN})_6$ ], respectively. The error of the ratio of Cr to CN for the materials prepared under same electrochemical conditions was  $\pm 4\%$  at maximum. The materials did not have as pure and well-defined a structure as would a single crystal.  
 12. K. Nakamoto, Ed., *Infrared and Raman Spectra of Inorganic and Coordination Compounds* (Wiley, New York, ed. 4, 1986).  
 13. The magnetizations at 5 T per unit cell of (a), (b), and (c) were 2.0, 1.8, and 2.6  $\mu_B$ , respectively, whereas the saturation magnetizations expected from these formulas were 7.2, 2.6, and 5.7  $\mu_B$ , respectively. The first magnetization curves at 10 K showed that magnetization for (b) almost saturated at 5 T. The saturation magnetization of (b), 1.8  $\mu_B$  per unit cell, was relatively close to the 2.6  $\mu_B$  expected from the unit cell formula. The low saturation magnetization could be explained by the existence of a relatively large amount of  $\text{Cr}^{\text{II}}\text{-CN-Cr}^{\text{III}}$  moieties, in which the spins of the *d* or-

bital canceled out each other. On the other hand, the magnetization curves for (a) and (c) still increased at around 5 T, and the magnetizations obtained at 5 T for (a) and (c) were fairly small compared with saturation magnetization expected from their formulas. However, it seems that such small values are often observed for chromium cyanide magnets. Mallah *et al.* (4), for example, reported 1.4  $\mu_B$  at 7 T, instead of the expected 6  $\mu_B$ , for  $\text{Cr}_5(\text{CN})_{12}$  ( $T_c = 240\text{ K}$ ).  
 14. The FT-IR spectra obtained before and after the electrochemical reduction showed that the absorption coefficient of CN at  $2071\text{ cm}^{-1}$  was about 1.7 times as large as that at  $2187\text{ cm}^{-1}$ . Considering the relative absorption coefficient of the CN stretching peaks and the IR spectra in Fig. 2, the ratio of  $\text{Cr}^{\text{II}}$  to  $\text{Cr}^{\text{III}}$  coordinated to the carbon in (b) could be estimated to be 0.80:0.20, that is,  $\text{Cr}_{0.16}^{\text{II}}(\text{high-spin})\text{Cr}_{0.96}^{\text{III}}(\text{low-spin})\text{Cr}_{0.80}^{\text{III}}(\text{CN})_6$ .  
 15. Electrically tunable magnets are proposed here to be designated as "electromagnetic materials" by analogy with the term "electrochromism."  
 16. We thank H. Etoh and J. Ichihayagi for their support in these experiments and D. Tryk for reading the manuscript.

22 May 1995; accepted 13 November 1995

## Achieving Linear Scaling for the Electronic Quantum Coulomb Problem

Matthew C. Strain, Gustavo E. Scuseria,\* Michael J. Frisch

The computation of the electron-electron Coulomb interaction is one of the limiting factors in ab initio electronic structure calculations. The computational requirements for calculating the Coulomb term with commonly used analytic integration techniques between Gaussian functions prohibit electronic structure calculations of large molecules and other nanosystems. Here, it is shown that a generalization of the fast multipole method to Gaussian charge distributions dramatically reduces the computational requirements of the electronic quantum Coulomb problem. Benchmark calculations on graphitic sheets containing more than 400 atoms show near linear scaling together with high speed and accuracy.

Although first-principles electronic structure calculations of molecules have become routine, they remain limited to systems of modest size because of their steep computational cost. The electronic Coulomb problem, which scales quadratically with system size, is one of the fundamental obstacles in the quest for ab initio computations of large molecules. In this report, we present quantitative evidence demonstrating that a generalization of the fast multipole method (FMM) (1–3) to Gaussian charge distributions achieves near-linear scaling for the quantum Coulomb problem. The method, the accuracy of which we have tuned to machine precision in specific cases, becomes faster than standard analytic evaluation of Gaussian two-electron integrals for systems containing as few as 300 basis func-

tions. Our method integrates concepts recently introduced by others (4, 5) with unique elements as described below.

In the FMM, the system under consideration is embedded in a hierarchy of  $8^n$  ( $n < 7$  in this work) cubic boxes at the finest mesh level, where  $n$  specifies the total number of tiers. All charge distributions located in a given box are represented by multipole expansions about the center of the box. For highly accurate results, the near-field (NF) portion of the problem, which is defined by interactions inside a given box and neighboring boxes, is treated exactly. Interactions in the far-field (FF) are treated through multipole expansions. The distinctive characteristic of the FMM is that translation techniques allow these multipole expansions to interact at different mesh levels (depending on the distance between their centers) through an upward and downward pass of the tree hierarchy, yielding a method with effective linear scaling (2).

Crucial to the generalization of the Greengard-Rohklin algorithm (1, 2) to the quantum Coulomb problem is the defini-

tion of range or spatial extent of a continuum charge distribution. For Gaussian functions (4), the range definition can be derived from the basic Coulomb integral between two s-type distributions (6) as

$$\tau = (2s)^{-1/2} \text{Erfc}^{-1}(\epsilon) \quad (1)$$

where  $s$  is the exponent of the product Gaussian distribution,  $\text{Erfc}^{-1}$  is the inverse of the complementary error function, and  $\epsilon$  is the desired error in the approximation. The real number  $\tau$  is rounded up to the nearest integer, thus guaranteeing an error smaller than  $\epsilon$  per interaction (7). In our Gaussian FMM (GFMM) implementation, a given interaction is included in the FF only if the number of boxes separating the edge of the boxes containing the two charge distributions is larger than the sum of the ranges of the distributions; for the results presented in this report, this number is at least two boxes. The electron-electron NF interactions were treated exactly through six-dimensional analytic integration of Gaussian functions. We also truncated the maximum  $l$  ( $l_{\text{max}}$ ) of a given multipole expansion to an effective value  $l_{\text{eff}}$  based on

$$\epsilon = k(a/R)^{l_{\text{eff}}} \quad (2)$$

where  $\epsilon$  is the desired accuracy,  $a$  is a constant whose optimum value is 0.63, and  $k$  is adjusted such that  $l_{\text{eff}} = l_{\text{max}}$  when  $R = 3$  boxes. This simple formula is straightforward, substantially improves the speed of the GFMM (which asymptotically scales as  $l_{\text{max}}^4$ ), and still yields very accurate results. This approach, which shares the basic philosophy of the "very fast" FMM recently introduced for the point-charge case (5), is partially responsible for the good scaling properties of our method and is denoted GvFMM herein (7).

All computational developments and calculations reported here were carried out with a development version of the Gaussian suite

M. C. Strain and G. E. Scuseria, Center for Nanoscale Science and Technology, Rice Quantum Institute, and Department of Chemistry, MS 60, Rice University, Houston, TX 77005–1892, USA.

M. J. Frisch, Lorentzian, Inc., 140 Washington Avenue, North Haven, CT 06473, USA.

\*To whom correspondence should be addressed.